Structural basis for regulation and higher order assembly of human phosphofructokinase-1

Tanushri Kumar

A thesis

submitted in partial fulfillment of the

requirements for the degree of

Master of Science

University of Washington

2022

Committee:

Justin Kollman

Suzanne Hoppins

Kelly Lee

Program Authorized to Offer Degree:

Department of Biochemistry

University of Washington

Abstract

Structural basis for regulation and higher order assembly of human phosphofructokinase-1

Tanushri Kumar

Chair of the Supervisory Committee:
Justin Kollman
Biochemistry

Phosphofructokinase-1 (PFK-1) is a key regulatory enzyme in the glycolytic pathway that catalyzes the ATP-dependent phosphorylation of fructose-6-phosphate (F6P) to generate fructose-1,6-bisphosphate (F16BP). The reaction PFK1 catalyzes is irreversible and marks the committed step in glycolysis. As the major regulator of glycolysis, PFK-1 is extensively regulated by several allosteric effectors to control glycolytic flux in the cell. Humans have three genes that encode the PFK1 muscle (PFKM), platelet (PFKP), and liver (PFKL) isozymes. Each isozyme has distinct roles in their respective tissues leading to different regulatory and kinetic properties. Due to a lack of structural data surrounding the human isoforms of PFK-1, the molecular mechanisms underlying these functional differences among PFK-1 isoforms have not

been determined. In this work, I employed cryo-electron microscopy (cryo-EM) to study the structural basis of regulation of the PFK-1 isozymes. I solved high resolution structures of both PFKL and PFKM in functionally important liganded states. These structures show both isoforms can form filaments, and that PFKL C-terminus positioning assists in stabilizing the inactive state. Additionally, the inactive PFKL structure revealed multiple inhibitory ATP binding sites.

TABLE OF CONTENTS

LIST OF FIGURES

ACKNOWLEDGEMENTS

I'd like to thank all my family, friends, and mentors who have gotten me to this point in graduate school. While I didn't expect my graduate school journey to end this soon, I'm incredibly grateful and humbled by how much I learned during my time in this program. I've truly become a better scientist, teacher, and learner from this experience. I'd like to say thank you to all the members of the Kollman Lab for having me, I've learned so much from each of you. Thank you to Justin Kollman for being my mentor and for your constant support during my time in your lab.

Thank you to Mom and Dad for cheering me on no matter what, and for listening to me describe all my experiments in excruciating detail whenever I called. Thank you to my brother, Aaditya, for reminding me to do things for myself and to have fun every now and then. Thank you to my dear friends, Shirley Wong and Shauna Otto for your unwavering support and believing in me as I navigated grad school. I'd also like to thank my two cohort members, Audrey O'Neill and Richard Muniz for always making me laugh in the lab and for all the fond memories.

DEDICATION

I'm dedicating this thesis to all the women in my family who have broken gender norms and have trailblazed the path to higher education. Without you, I wouldn't be here to become the first woman in our family to attain a higher education science degree. Thank you.

Chapter 1. INTRODUCTION

1.1 Glycolysis and PFK-1

Glycolysis is an ancient and conserved pathway in which energy is extracted from the breakdown of glucose into pyruvate (**Figure 1**). In addition to the generation of pyruvate, glycolysis also produces anabolic intermediates that are used in other metabolic pathways, such as the Pentose Phosphate Pathway (PPP) and the Hexosamine Biosynthetic Pathway (HBP). Glycolysis is also vital to human health, as mutations in pathway enzymes lead to metabolic diseases[1,2], and many cancers rely on glycolysis for proliferation[3].

Phosphofructokinase-1 (PFK-1) is the key regulatory enzyme that catalyzes the rate-limiting step in the glycolytic pathway. In this step, fructose-6-phosphate (F6P) is converted to fructose-1,6-bisphosphate (F16BP) through the transfer of the gamma phosphate of ATP (**Figure 2**). As the major regulator of glycolysis, PFK-1 is tightly regulated to fine-tune flux in response to changing energetic demands. There are several allosteric effectors that influence the regulation of the enzyme; for example, at high concentrations ATP binding in allosteric sites inhibits PFK-1.

In humans, three genes encode PFK-1 liver, muscle, and platelet isozymes, which share 65% sequence identity. Each isoform has unique kinetics and sensitivities to allosteric regulators[4]. For example, muscle PFK1 (PFKM) is the most active isoform and is predominantly expressed in skeletal muscle where copious amounts of ATP are required. In contrast, liver PFK1 (PFKL) has a lower affinity for substrates and a higher sensitivity to ATP inhibition, which likely reflects a regulatory role related to the liver's function in maintaining blood glucose levels.

1.2 PFK-1 structure

The regulation and structure of bacterial homologs of PFK-1 have already been studied[5,6,7]. Bacterial PFK-1 takes the form of a tetramer composed of identical catalytic domains, as seen from the solved crystal structure of *Geobacillus stearothermophilus* PFK-1 in **Figure 3** (PDB: 4PFK). As seen in the crystal structure, the active site is formed by adjacent catalytic domains, where F6P and ADP are bound.

The human PFK-1 monomer consists of a regulatory and a catalytic domain, which then assembles into a tetramer (**Figure 4A).** The C-terminus lies between the catalytic and regulatory domains and has been reported to be involved in sensitivity to ATP inhibition of the enzyme[8]. Like bacterial homologs, the human PFK-1 active site is formed by adjacent catalytic domains. However, compared to prokaryotic PFK-1, eukaryotes have a more complicated quaternary structure. This is due to a gene duplication event[9], leading to the evolution of the regulatory domain in eukaryotes, adding new sites for effector binding. These allosteric effectors bind the regulatory domain to influence the equilibrium between active and inactive states (**Figure 4B**). There is also a conformation change present between the active and inactive states of the enzyme, where flexing between the catalytic and regulatory domains occurs.

1.3 PFKL filament formation

In recent years, biochemical and structural studies have revealed many different metabolic enzymes form filaments that add another level of regulation to enzyme activity[10,11,12,13]. The self-assembly of these polymers are often driven by changes in metabolites and flux in the cell. A recent study[14] from the Kollman Lab with our collaborator Brad Webb showed recombinant PFKL assembles into filaments. The PFKL filaments are composed of stacks of tetramers, connected by regulatory domains, indicating the filaments may have a role in regulation (**Figure 5A**). Filament

formation was induced upon addition of the substrate F6P but was not seen for the PFKP and PFKM isoforms (**Figure 5B**). In this study, the regulatory domain was shown to be required for filament formation using a chimera of the PFKP catalytic domain fused to the regulatory domain of PFKL, where light scattering experiments demonstrated filament assembly (**Figure 5C**). Structurally, the PFKL filaments also show a unique helical geometry. In a growing PFKL filament, there are two sites of addition for the next PFKL tetramer (**Figure 5D**). Depending on which site is bound, either a "straight" or a "kinked" filament will form, but the interface that is made remains the same.

1.4 Cryo-EM as a method to study allosteric regulation

Much of the data surrounding PFK-1 regulation come from bacterial homologs, as there is a lack of structural data surrounding the human isoforms. Crystal structures of PFKP exist[15], but they are locked in a single conformation despite the presence of different allosteric ligands. Cryo-EM functions as a robust tool to study conformational changes in response to allosteric binding, as the sample is actively turning over substrate as it is plunged frozen. In my thesis work, I used cryo-EM to solve functionally important liganded states of both PFKL and PFKM, and I provided insight into the structural basis of regulation of human PFK-1 through allosteric ATP binding, filament formation, and C-terminal tail binding.

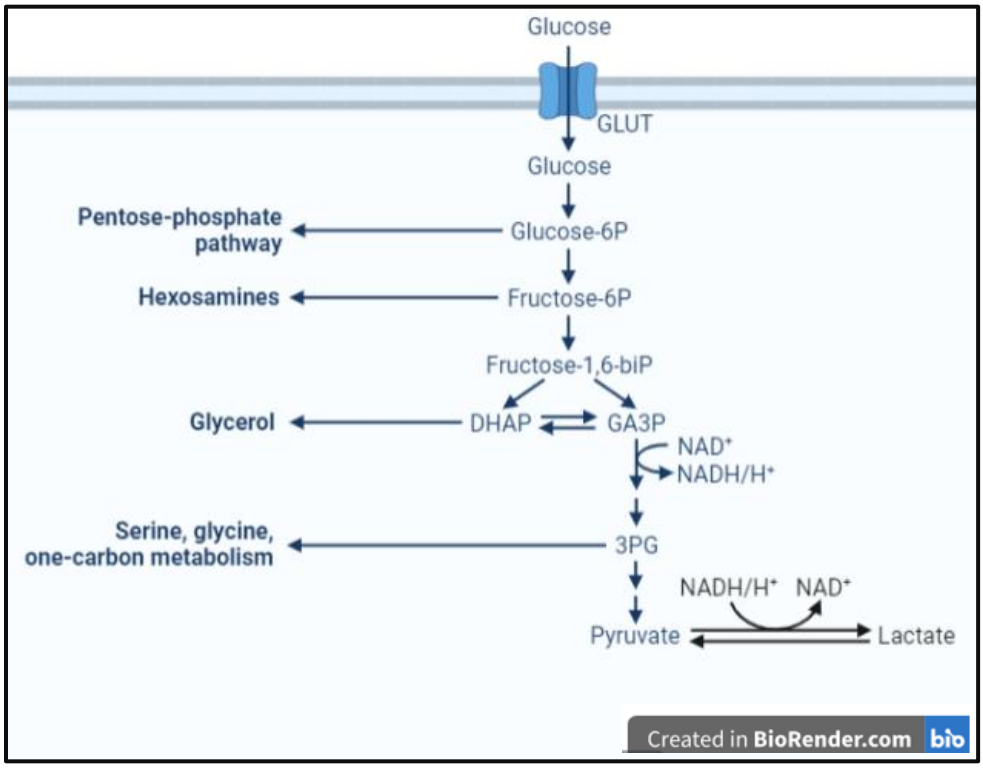

Figure 1. The Glycolytic Pathway. Glycolysis is the metabolic process in which glucose is broken down into pyruvate for further catabolism in the cell. This process produces energy in the form of ATP and NADH, as well as providing metabolic intermediates for other synthesis pathways.

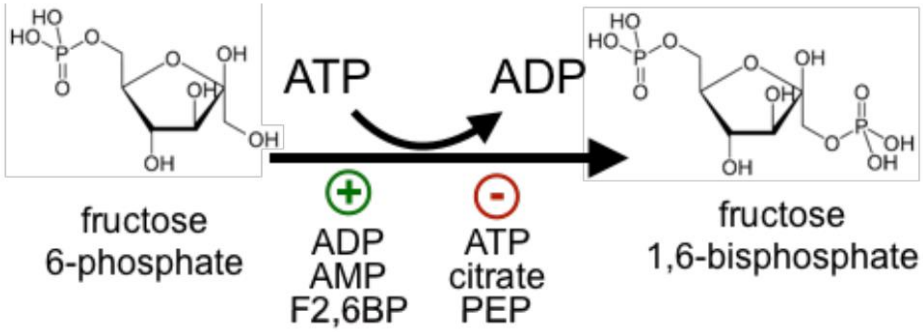

Figure 2: PFK-1 reaction. Phosphofructokinase-1 catalyzes the ATP dependent phosphorylation of fructose-6-phosphate to fructose-1,6-bisphosphate. This enzyme is allosterically regulated by many effectors. ADP, AMP, and F2,6BP act as activators, while ATP, citrate, and PEP act as inactivators.

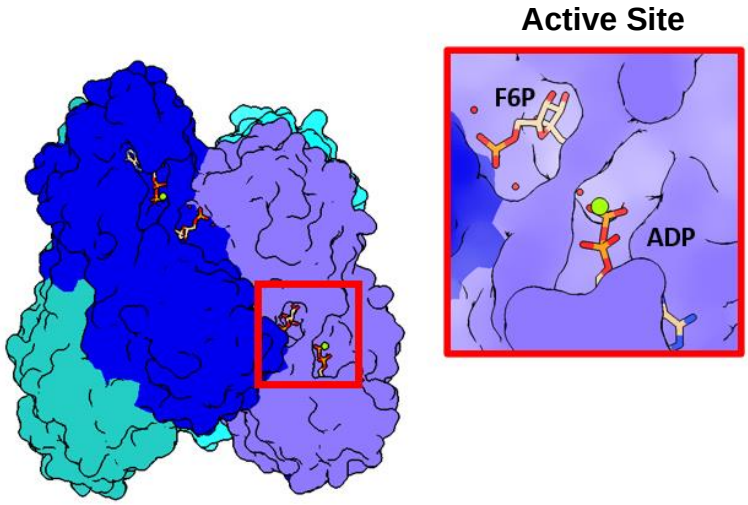

Figure 3: Bacterial PFK-1 Structure. Crystal structure of PFK-1 from of *Geobacillus stearothermophilus* (PDB: 4PFK). The tetramer is composed of four identical monomers. The active site is highlighted in red. Both F6P and ADP are bound in the active site of the enzyme.

4A)

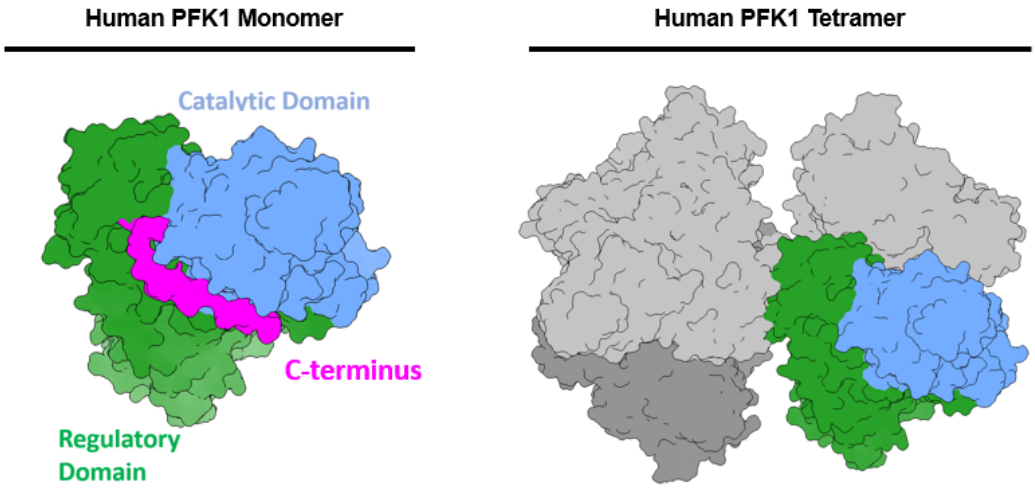

4B)

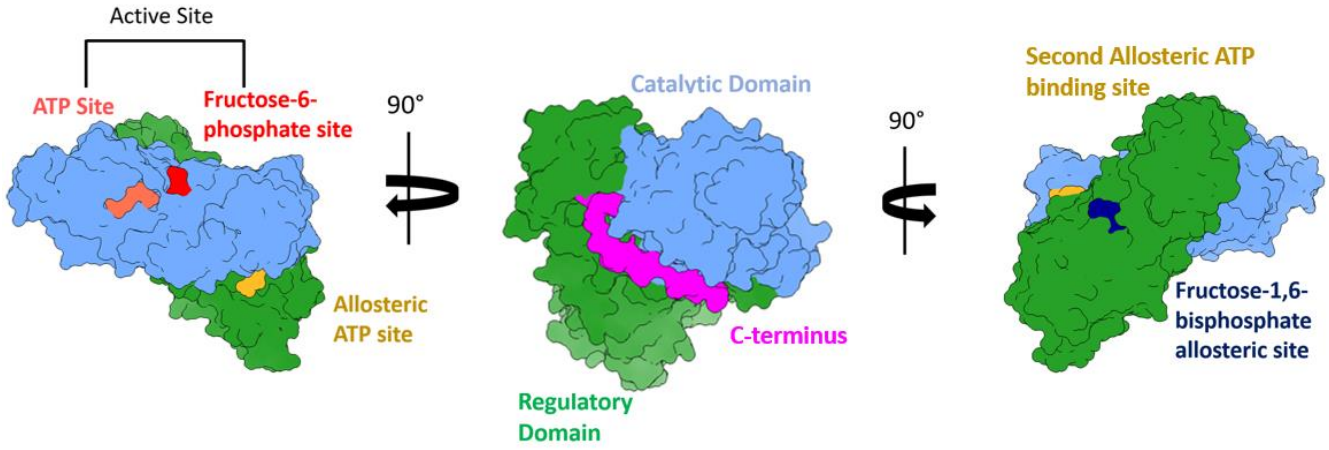

Figure 4: Human PFK-1 Structure. 4A: The human PFK-1 tetramer. The human PFK-1 monomer consists of an N-terminal catalytic domain (blue) and a C-terminal regulatory domain (green). The C-terminus (purple) lies between the two domains. Four copies of the monomer assemble into the PFK-1 tetramer. **4B: Front and side views of PFK-1 monomer.** The active site is shown where F6P (red) and the catalytic ATP (orange) bind. The allosteric ATP sites are shown in gold. The allosteric binding pocket for the product F16BP is highlighted in dark blue.

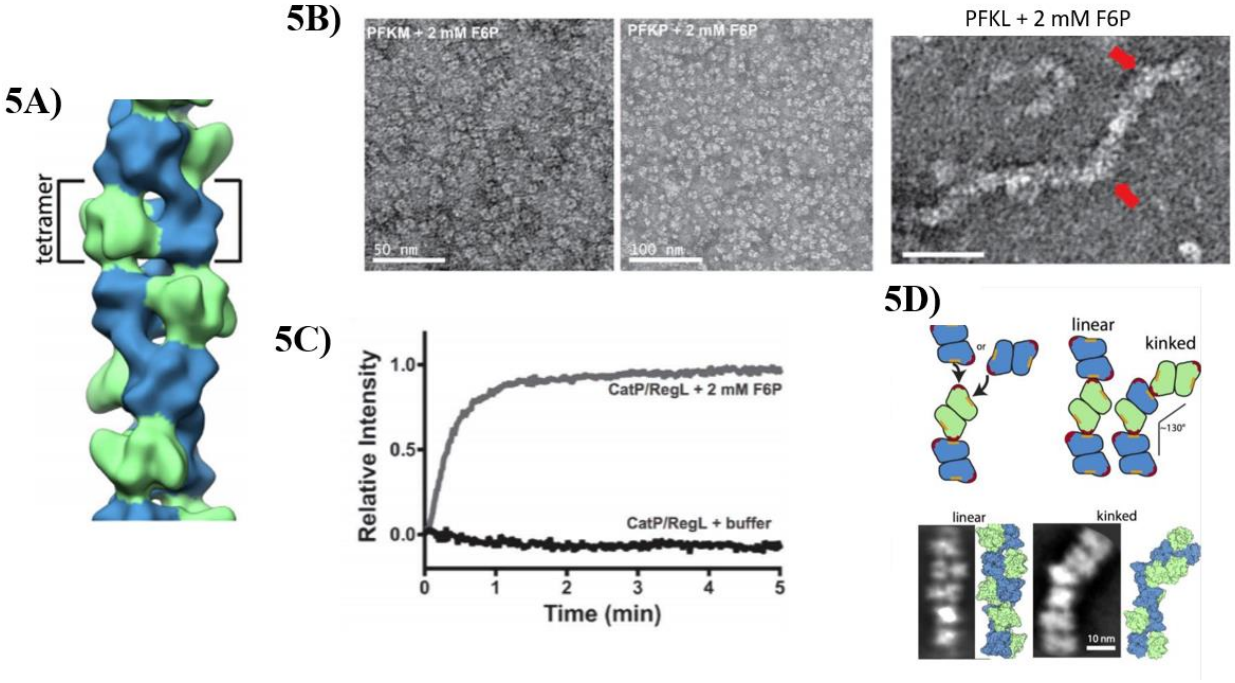

Figure 5: PFKL Filament Formation. 5A: Filaments are formed by stacks of tetramers, shown by a negative stain EM 3D reconstruction. **5B:** Upon addition of F6P, PFKL forms filaments. Red arrows point to kinks in the filament architecture. **5C:** Light scattering experiments show the regulatory domain of PFKL is required for filament formation. CatP/RegL refers to a chimera fusion of the catalytic domain of PFKP and the regulatory domain of PFKL. **5D:**

Negative stain averages show unique helical structure in the PFKL filaments, with the appearance of "kinked" and "straight" filaments. **(**Figure adapted from Webb et.al 2017**)**

Chapter 2. RESULTS

2.1 PFKL filaments in the active conformation

Previous work in our lab solved high resolution cryo-EM structures of PFKL bound to F6P and the activating drug NA11[16], which binds in the AMP/ADP activating site in the regulatory domain, to induce the active conformation of the enzyme. Cryo-EM structures for both the PFKL tetramer and filament were solved (**Figure 6**) to high resolution. These structures showed two interface contacts in the filament assembly. The first was the contact between regulatory domains previously reported by our group[14]. The second contact involved a loop region (residues 693-705 of the regulatory domain) dipping down into the catalytic domain of the tetramer below (highlighted in yellow in **Figure 6**). Lastly, density for the C-terminus was not seen under this liganded conditions, indicating that it was disordered.

2.2 PFKL filaments in the inactive conformation

To compliment the previously solved active conformation of the PFKL filament, I solved high resolution cryo-EM structures of the PFKL tetramer and filament in the inactive conformation. This condition was done at inhibitory concentrations of ATP (2 mM ATP[14]) along with the addition of the product, F16BP, to stabilize the tetramer. The PFKL tetramer went to 2.4 Å, while the filament went to 2.9 Å. The higher resolution inhibited PFKL filament structure shows hydrogen bonding and salt bridge interactions (**Figure 7A**) present at the site 1 interface. These are the same interactions present in the active filament as well, demonstrating that the site 1 interactions remain the same, despite conformational changes in the protomer. Strikingly, the inactive PFKL filament is missing the site 2 contact seen in the active conformation (**Figure 7B**).

The cryo-EM structure shows a resolved C-terminus (**Figure 7B**) that is bound back against the enzyme and blocks the secondary contact from being made. This data indicated that the inactive conformation is stabilized by C-terminus positioning, and that the site 2 contact is inhibited by C-terminal binding (**Figure 8**).

2.3 Inactive PFKL allosteric binding of ATP

Allosteric inhibition by ATP is well documented as a method of regulation of PFK-1 activity[17]. The literature shows two inhibitory allosteric ATP binding sites for PFK-1, where the secondary allosteric ATP binding site (**Figure 4B**) has been noted in other homologs[5,18] but has not been demonstrated in the human PFK-1 isozymes. My high resolution cryo-EM structures for both the PFKL tetramer and filament show the second allosteric ATP site, as well as the binding pocket (**Figure 9)**. The structure reveals a different pose of the bound ATP compared to previously solved structures. It is unknown if ATP binds in this site in the other human isoforms, but sequence conservation suggests most of the residues in this binding pocket are conserved (**Figure 10**).

2.4 Expression of PFKL in human Expi293F cells

For all cryo-EM related studies, we have used prepared PFK-1 protein that was generously provided from our collaborator, Brad Webb. These protein preps were purified using a baculovirus system in insect cells[14]. To address the function of filaments in the context of human cells, as well as to address the effects of PTMs, I developed an expression system in human Expi293F cells for PFKL. Time course experiments of PFKL expression revealed the optimal amount of protein could be harvested 3 days post transfection (**Figure 11A**). Subsequent protein purification yielded pure PFKL protein post size-exclusion (**Figure 11B**). Negative-stain EM of the protein prep confirmed proper quaternary structure of the human cell-expressed PFKL. Due to the low final concentration of the protein prep (0.1 mg/mL), the critical concentration for tetramers were not reached, leading

to the appearance of a mixed population of monomers, dimers, and tetramers (**Figure 11C**). Future work will need to involve upscaling the protein prep to maximize the final concentration of protein.

2.5 Allosteric regulation of PFKM

To see if the structural regulation observed in PFKL was conserved across the different human PFK-1 isoforms, I solved a cryo-EM structure of PFKM under similar conditions of the inactive PFKL structure (1.7 mM ATP, with F16BP added). The resulting structure went to 3.4 Å (**Figure 12A**) and revealed three important discoveries. First, assembly contacts could be seen in the 2D class averages (**Figure 12B**), indicating filament formation for PFKM. Using 3D classification, I could pull out the filament class for PFKM, although it did not go to high resolution as filament formation was not robust. Second, the second allosteric site seen in the inactive PFKL structure only showed partial density, indicating partial binding of ATP in that site (**Figure 12C**). Lastly, the C-terminus showed no density, like the active PFKL structure. Indeed, upon visual inspection of the conformation compared to the solved PFKL models, there does appear to be more similarity to the active conformation of PFKL (**Figures 12D and 12E**). These data indicate that the inactive conditions used for PFKL do not necessarily inactivate PFKM.

2.6 pH sensitivity of PFKM

Upon further research[19,20] it was found that previous studies have found that PFKM is pH sensitive in its activity (all cryo-EM grids had been prepared at pH 7.5 at this point). Our collaborator, Brad Webb, had found in previous experiments that PFKM was completely inactive at conditions of 4 mM ATP, 0.5 mM F6P, at pH 6.8[20]. To understand what was occurring structurally, I froze cryo-EM grids of PFKM with this condition, with the change of F6P concentration to 0.25 mM to favor the inactive state and collected a dataset. The cryo-EM dataset revealed PFKM was breaking into dimer structures, which could be seen from the 2D class

averages (**Figure 13A**). Using 3D reconstruction in Cryosparc, a low-resolution map could be generated for this dimer structure (**Figure 13B**), although more particles would be needed to push to high resolution. Previous work solved a rabbit muscle PFK-1 crystal structure under conditions of F6P, ADP, and F26BP with a pH of 5.3. Despite the presence of activating compounds, the authors also noted a dissociated dimer structure (**Figure 13C**), like the human PFKM structure in **Figure 13B**. While authors suggest the dimerization is the result of the low pH required for crystallization, the fact that it is seen in the cryo-EM structure informs us this is a real solution dimer rather than an artifact.

2.7 The second allosteric ATP binding site as a pH sensor

It is already known that PFKM is inactive in the dimeric form[4], as the active site is unable to form without the tetramer. However, previous crystallographic studies with rabbit muscle PFK[18] done at low pH also show a dimeric structure also show the second allosteric ATP binding site occupied. This could indicate the role of the second allosteric ATP binding site as a pH sensor, to trigger the dissociation into dimers at lower pH. As a preliminary screen, I used negative stain-EM to screen different pH conditions and ATP concentrations for PFKM to understand what was triggering the dissociation into dimers. From the negative stain screen (**Figure 14A**), only with high concentrations of ATP at low pH is the dimeric PFKM seen. This supports the theory of the secondary allosteric ATP site getting occupied at high ATP concentrations, leading to the dissociation into dimers at low pH. Interestingly, upon addition of the product, F16BP, the tetramer form of PFKM is rescued under the high ATP and low pH condition (**Figure 14B**).

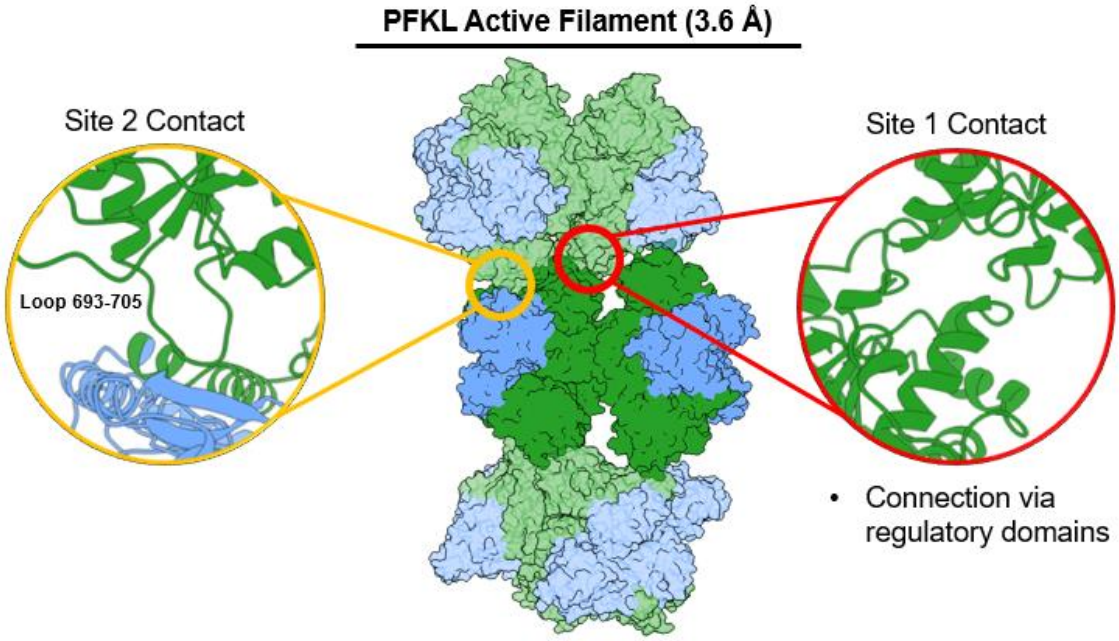

Figure 6: PFKL Filament in the active conformation. The cryo-EM reconstruction of the PFKL filament is colored by domains, blue is the catalytic domains, green is the regulatory domains. This structure went to 3.6 Å. Ligands that are bound in this structure include ATP, NA11, and F6P. The site one contact (red) shows the main filament interface is composed of interactions between regulatory domains. The site two contact (yellow) shows a loop of the regulatory domain (Loop 693-705) dipping down into the catalytic domain of the next subunit down. The C-terminus in this structure is also disordered.

7A)

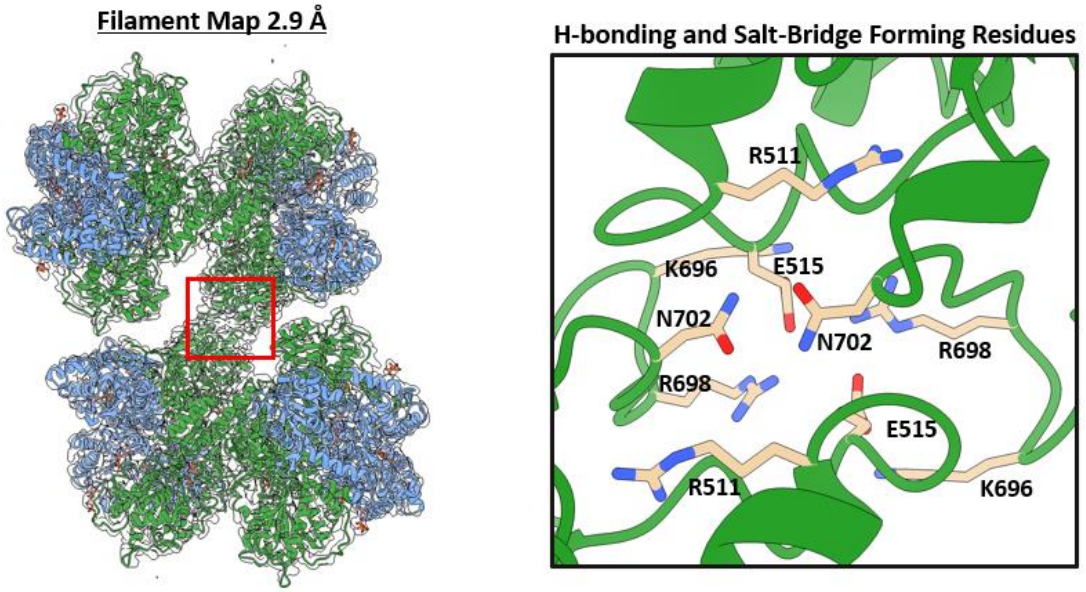

7B)

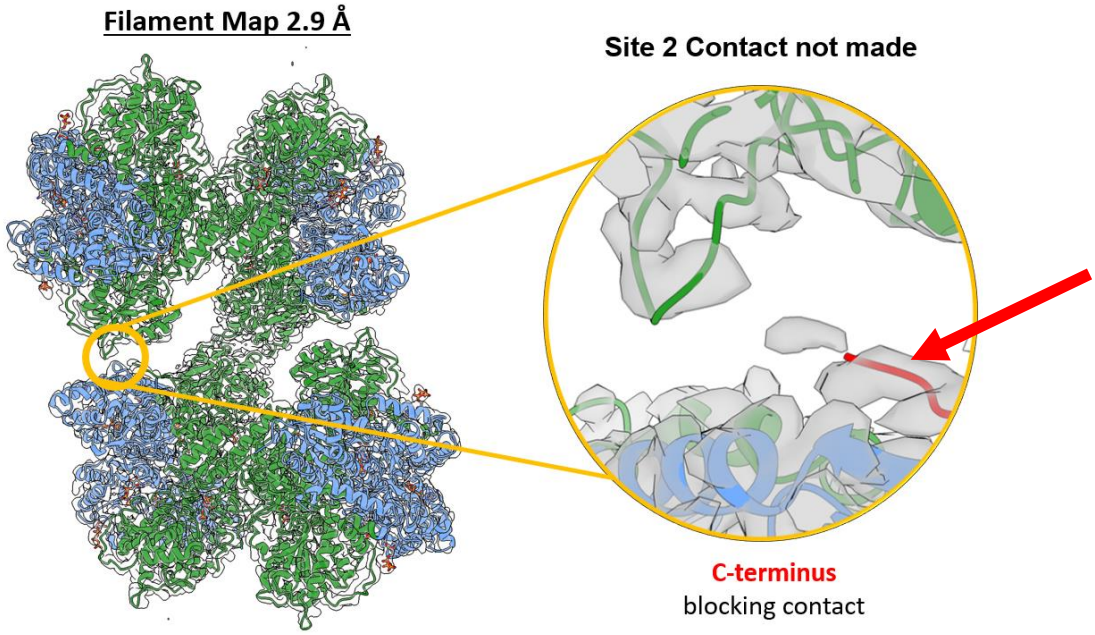

Figure 7: The inactive PFKL filament shows one interface contact. 7A) PFKL filament model with cryo-EM density, with a resolution of 2.9 Å. The filament model is colored by domain, where blue is the catalytic domains and green are the regulatory domains. The inset shows the salt bridge and hydrogen bonding interaction present at the site 1 contact. **7B) The site two contact is not made in the inactive filament.** Highlighted in yellow is where the second contact appears in the active conformation. The inset shows the filament model with the cryo-EM density, where the C-terminus (in red) is shown to be blocking the site 2 contact.

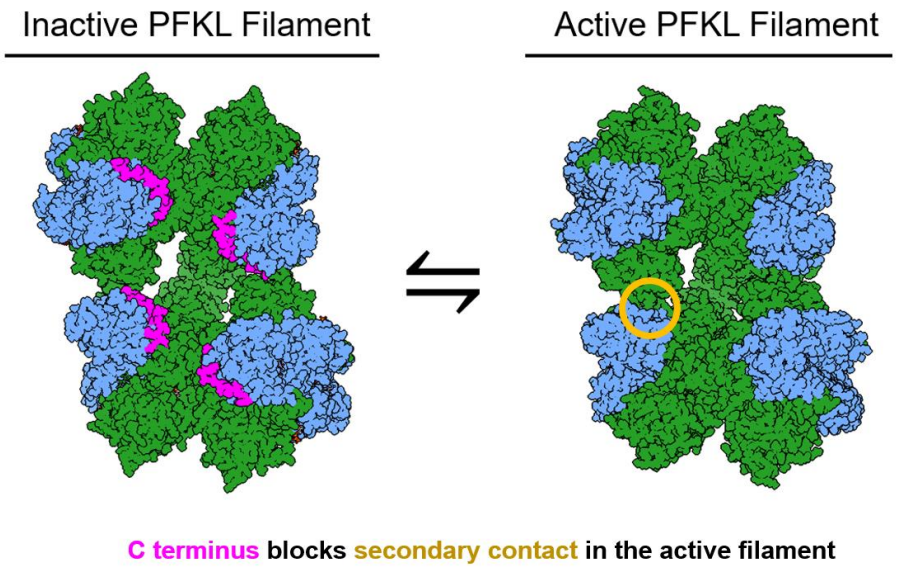

Figure 8: C-terminal binding stabilizes the inactive PFKL Filament. Catalytic domains are blue and regulatory domains are green. The C-terminus is highlighted in purple, and site 2 contact is circled in yellow. Upon the conformation change into the active state, the C-terminus is displaced, and the secondary contact is made.

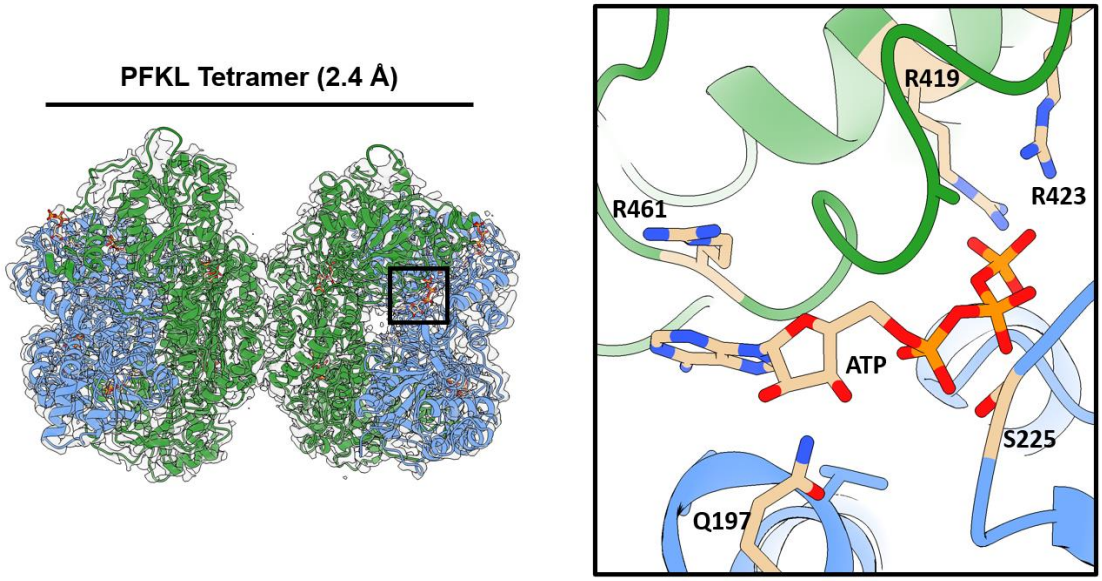

Figure 9: Inactive PFKL structure reveals second allosteric ATP binding site. PFKL tetramer density map is shown above with the atomic model, at 2.4 Å resolution. The inset shows the ATP binding pocket, located between the catalytic (blue) and regulatory (green) domains.

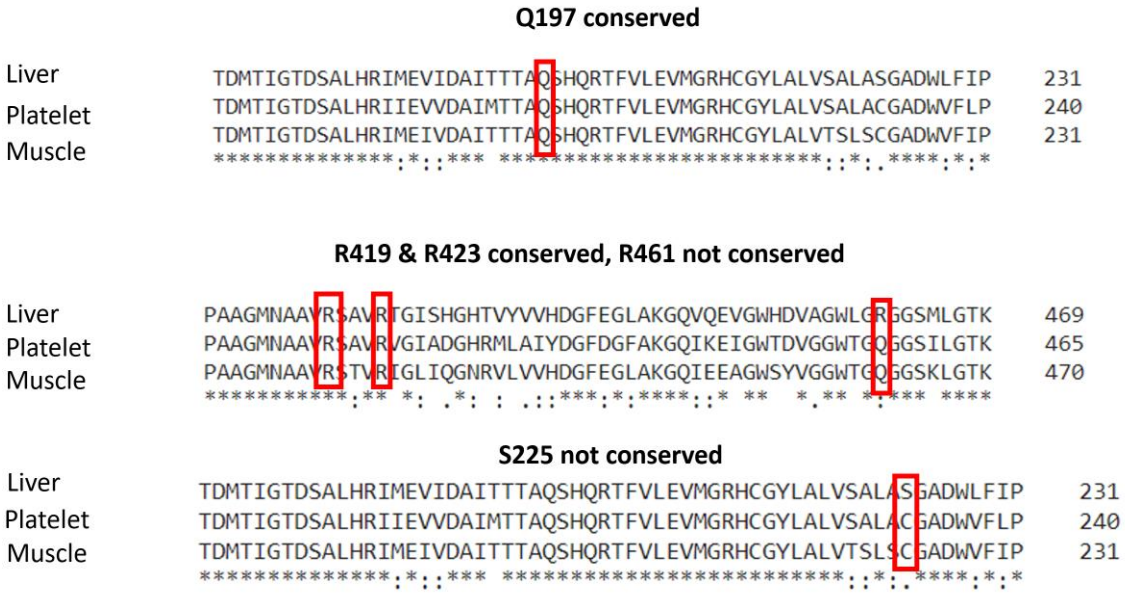

Figure 10: Sequence alignment shows ATP binding pocket is mostly conserved. Amino acid sequence comparison between the human liver, platelet, and muscle PFK-1 isoforms. Highlighted in red are the residues involved in the ATP binding pocket. Of the five, only R461 and S225 are not conserved. Sequence analysis was done using Clustal Omega.

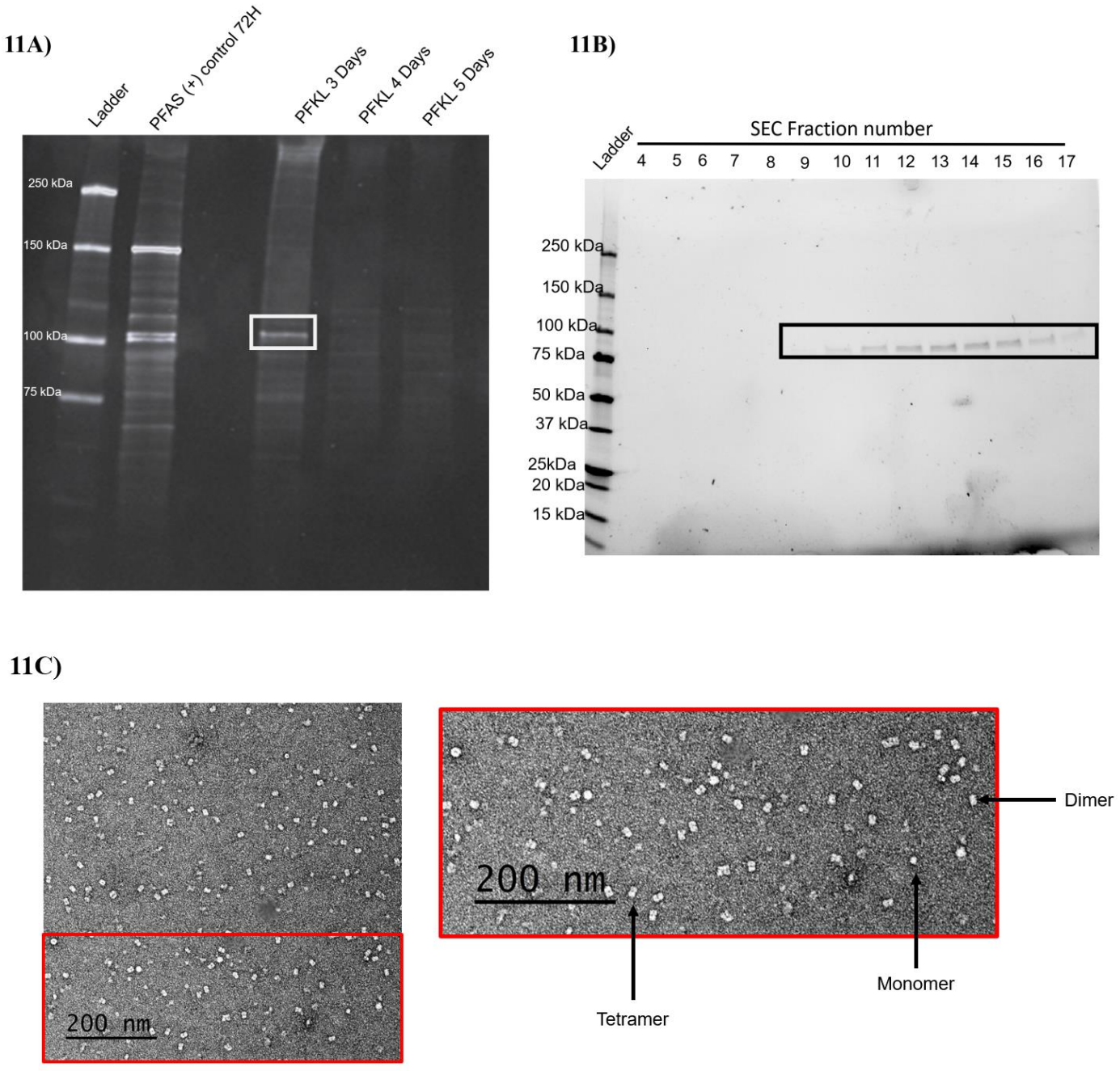

Figure 11: Expression and Purification of PFKL in human Expi293F cells. 11A) Western blot of whole cell lysate of Expi293F cells expressing PFKL or the positive control PFAS. Time course for PFKL occurred over 5 days post transfection, where cell lysate harvested on day 3 had the most signal of PFKL expression (highlighted with white box). **11B)** SDS-PAGE gel run post size exclusion chromatography (SEC). Fraction 8-17 was pooled together and concentrated, as they had the expected weight of PFKL, 85 kDa. **11C)** Negative stain-EM of PFKL purified from Expi293F cells. Protein concentration on the grid was at 120 nM. Indicated on the inset are the presence of monomer, dimers, and tetramers in the sample.

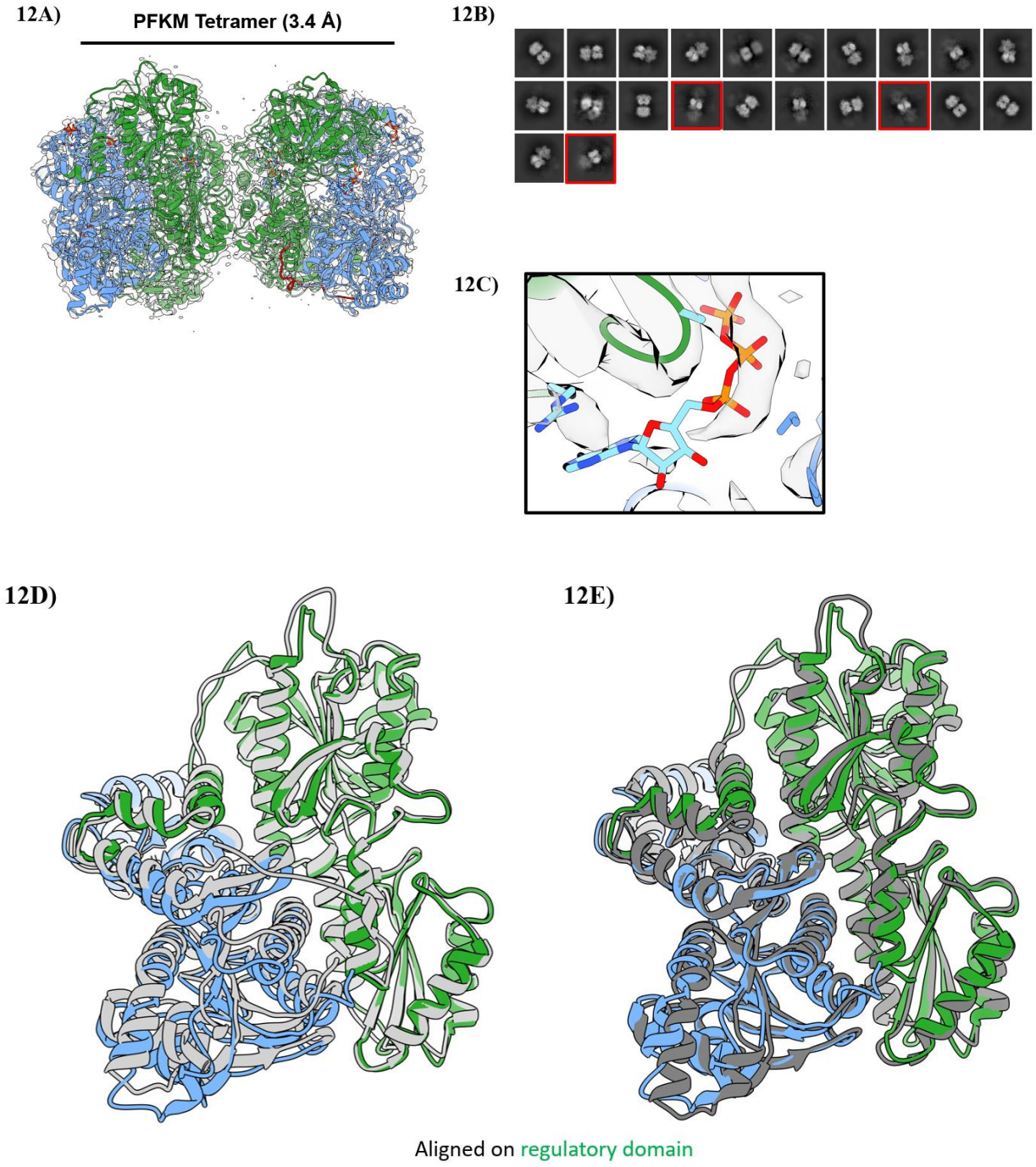

Figure 12: PFKM displays different structural regulation than PFKL. 12A) PFKM density map (3.4 Å resolution) with the inactive PFKL atomic model docked. Blue domains are catalytic, and green are regulatory. **12B)** Cryosparc 2D class averages. Classes that show assembly contacts are highlighted in red. **12C)** Second allosteric ATP site for PFKM with partial density shown. **12D)** Alignment of domain docked PFKM monomer with the inactive PFKL atomic model. The PFKM model is colored by domain, while the PFKL model is shown in light grey. RMSD between the two structures is 1.4 Å. **12E)** Alignment of domain docked PFKM monomer with active PFKL atomic model (dark grey). RMSD between the two structures is 1.7 Å. Both models in 12D and 12E are aligned on the regulatory domain (residues 361-768) of the PFKM model.

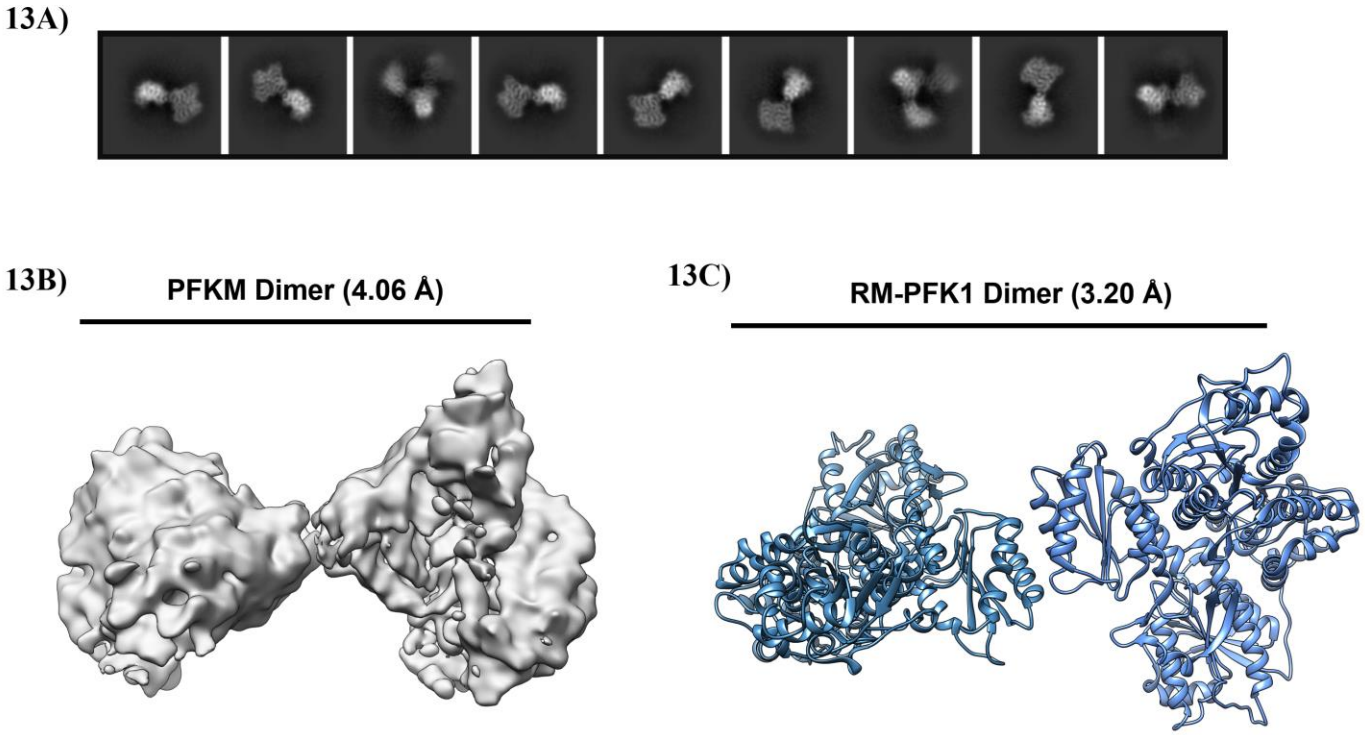

Figure 13: PFKM dissociates into dimers at low pH and high ATP concentrations. 13A) Cryosparc 2D class averages of PFKM dimer. **13B)** Cryosparc 3D reconstruction of PFKM dimer, consisting of 66,704 particles. **13C)** Rabbit Muscle PFK1 (RM-PFK1), PDB: 3O8L. Under low pH conditions, RM-PFK1 also dissociates into dimers like the human PFKM in 13C. Each chain is colored a different shade of blue.

14A)

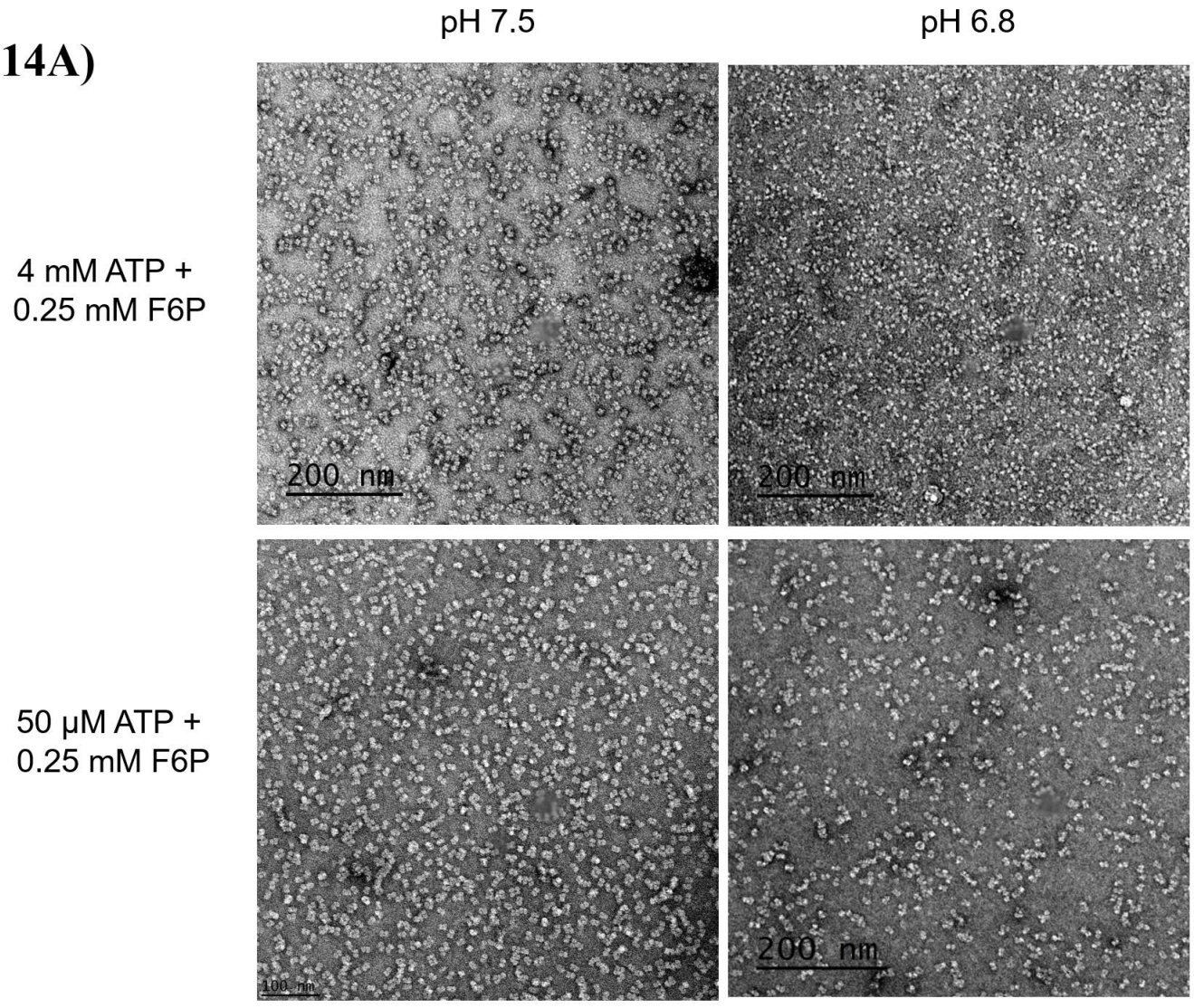
pH 7.5
pH 6.8
4 mM ATP +
0.25 mM F6P
50 µM ATP +
0.25 mM F6P
200 nm
200 nm
100 nm
200 nm

14B)

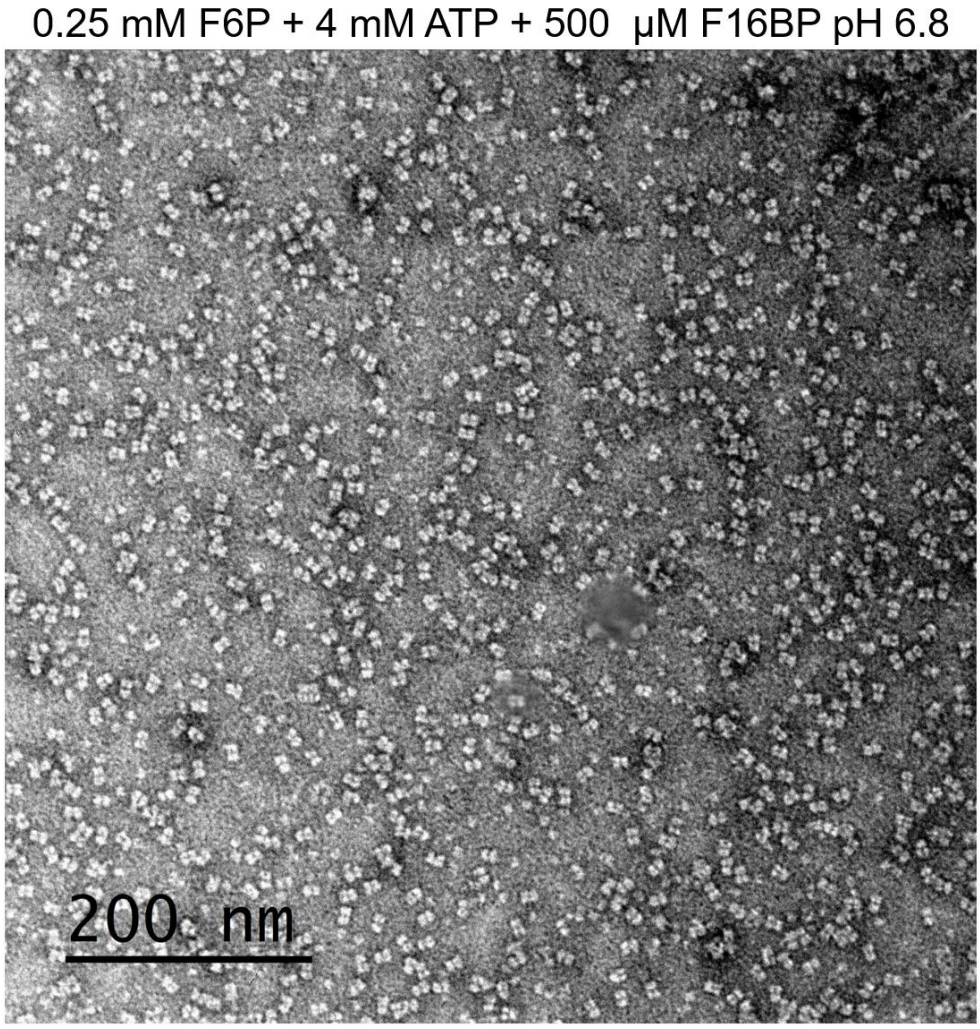

Figure 14: PFKM structural organization is highly dependent on both pH and ATP concentrations. 14A) Negative stain-EM images of PFKM under varying pH and ATP concentrations. All negative stain-EM grids were prepared at 600 nM protein concentration. Only the 4 mM ATP, 0.25 mM F6P at pH 6.8 yields dissociation of the tetramer. **14B)** Negative stain-EM shows rescue of the PFKM tetramer from the the 4 mM ATP, 0.25 mM F6P at pH 6.8 condition upon addition of F16BP.

Chapter 3. DISCUSSION

3.1 The role of PFK-1 filaments in regulation

From my thesis work, we can see that PFKL filaments add a structural level of regulation to the enzyme. My inactive PFKL filament structure demonstrated only one filament interface contact and a resolved C-terminus. Upon the conformational change to the active state, there is C-terminal tail destabilization, and a secondary contact made in the filament. The mechanism of C-terminal disruption in the filament points to a possible role of cooperativity of the filaments. Activating one tetramer in a PFKL filament can lead to a cascade effect, in which subsequent tetramers connected in the filament are activated through conformational changes induced by the site 2 contact. Cooperativity by filament formation has also been documented for other metabolic enzymes, such as CTP synthase 2[21].

Future work can look at using the high resolution cryo-EM structures to design mutations that break filament assembly and test the effects on PFKL enzyme activity. Upon inspection of the site 1 interface, mutating N702 to an alanine would break a core hydrogen bonding interaction with the N702 interaction from the second protomer (**Figure 7A**). To investigate the effect of the site 2 contact on cooperativity, mutations on the site 2 contact loop (residues 693-705) could be made. However, it should be noted that the residues involved in the site 2 contact are also involved in the site 1 contact for a different protomer. In other words, there is a risk of breaking the site 1 contact with site 2 contact mutations. Another approach would be to make mutations to the regions of the catalytic domain to which the site 2 contact loop binds to.

From my thesis work, it is also clear that PFKL is not the only isoform capable of forming filaments. PFKM filaments, although not robust, were seen in my cryo-EM datasets (**Figure 12B**). This begs the question of whether the regulation conferred by filament formation is conserved

between the PFK-1 isoforms. In the future, experiments should be done to understand what causes filament formation for PFKM, and if the structural organization of the filaments are like PFKL. Future work should also look at potential PFKP filament formation. While previous work did not note PFKP filament formation[14], it is possible that under different metabolic conditions the enzyme could also form higher order structures.

3.2 The role C-terminal tail regulation

My thesis work provided strong support for the C-terminal tail as another mode of structural regulation for PFKL. The C-terminus has already been documented to be important for the regulation of the enzyme[8]. This makes sense, considering the C-terminus lies between the catalytic and regulatory domains, where it is maximally sensitive to conformational changes in the protomer. Previous work[8] found L767 and E768 to be functionally important residues in the C-terminal tail to maintain sensitivity to ATP inhibition for PFKM. At the time this paper was published, there was not a structural understanding yet as to why this was the case. This led the authors to speculate these mutations prevented the conformational change to the inactive state. With our cryo-EM structures, we are now aware that the C-terminus is bound back against the structure in the inactive conformation, and disruption of the C-terminal tail is associated with the active conformation. Using the inactive PFKL structure, future work can use the resolved C-terminus to make point mutations on the tail, including L767 and E768, to test the effect of sensitivity to ATP inhibition.

3.3 The role of the second allosteric ATP binding pocket

The inactive PFKL filament and tetramer structures revealed a second allosteric ATP binding site, located between the catalytic and regulatory domains. While this site has been noted in other homologs, it has yet to be seen in a human structure. Additionally, the pose in which the

ATP is bound in the inactive PFKL structure appears to be novel. With the high resolution inactive PFKL structures, we can see what the binding pocket looks like, and which residues are involved in ATP binding. Mutations can be made to disrupt the ATP binding in this pocket, and to assess the impact this will have on ATP inhibition of the enzyme. The sequence conservation of the binding pocket (**Figure 10**) suggests this site exists in the other human isoforms. For the PFKM tetramer structure there is partial density for this ATP binding site (**Figure 12C**), indicating the PFKM is also capable of binding ATP in this site.

3.4 The effect of pH on PFKM quaternary structure

My work with PFKM uncovered different levels of structural regulation based on pH. The initial PFKM structure I solved (**Figure 12A**) was performed under similar inactivating conditions as PFKL, as well as physiological pH (pH: 7.5). Structurally, the enzyme did not maintain the same elements as PFKL in inactivating conditions, of note was the lack of C-terminal tail binding and the partial density for ATP in the second allosteric site. Upon further research and discussion with our collaborator, we found that PFKM is specifically inhibited at low pH (pH: 6.8). Re-doing the cryo-EM data collection at a much higher ATP concentration (4 mM) and at pH:6.8, PFKM dissociated into dimers (**Figures 13A and 13B**). A similar structure has been deposited in the PDB (3O8L), for rabbit muscle PFK. The authors claim the dimer structure is a crystallographic artifact, as the pH had to be dropped to pH 5 to crystallize the protein. Even more, the dimer rabbit muscle structure shows the second allosteric ATP site occupied by a phosphate group. This points to some type of functional relevance of the dimerization effect with the occupation of the second allosteric ATP site at low pH. Future work should look at optimizing the PFKM dimer cryo-EM structure by collecting a larger dataset to attain a higher resolution reconstruction to see if the second allosteric ATP site is occupied.

In further support of the second allosteric ATP site triggering the dimerization of PFKM, I performed a negative stain-EM screen with different combinations of pH and ATP concentration (**Figure 14A**). These negative stain experiments confirm that high ATP concentrations are what drive PFKM into dimers at low pH, as at low ATP concentrations (50 μM) and low pH, there are still tetramers present. This supports the notion of the second allosteric ATP site as a pH sensitive site, where occupation of the site triggers the dimerization effect for PFKM. My experiments also demonstrate the change between tetramers and dimers is dynamic, as upon addition of the product (F16BP) the tetramers are rescued for PFKM (**Figure 14B**).

The pH mechanism of inactivation for PFKM serves as a mode of protection in the muscle, as a decrease in pH is seen during anerobic metabolism. By inactivating the enzyme when the pH drops, the muscle is protected from the effects of built-up acidification[22]. Whether PFKL or PFKP are pH sensitive as well remains to be seen, as the pH sensitivity has been most documented with PFKM.

Chapter 4. CONCLUSION

My thesis work has provided significant insight into how filament formation, C-terminal tail binding, and allosteric ATP binding all influence regulation of PFK-1. Even more, my work has made connections between pH and allosteric binding of ATP for PFKM, along with a possible mechanism for regulation. However, without functional studies it is hard to confidently say the true function of these structural elements of the enzyme. Future work should investigate the role of filament formation on enzyme activity and *in vivo* to understand this regulation in a biological context. I have already setup the groundwork for potential *in vivo* experiments for PFKL using the Expi293F expression system, which could also be easily adapted to be used for the PFKM and

PFKP isoforms. With the combination of cryo-EM and biochemical studies, precise experimentation can be done to ascertain the structural basis of regulation for the human PFK-1 isoforms.

Chapter 5. METHODS

Cryo-EM

Cryo-EM samples were prepared on glow-discharged grids. Grids used for cryo-EM experiments were C-flat 2/2 holey carbon grids (Protochips Inc). Grids were blotted with Whatman filter paper 3 times (using 2.5 µL of sample for each blot) before loading onto Vitrobot for a final blot and subsequent ethane plunging. Vitrobot blotting was performed at 100% humidity, at room temperature, with 0 blot force and waiting time. Grids were immediately clipped and stored in a large liquid nitrogen dewar after freezing. Samples for cryo-EM were performed at 10 µM enzyme. For the inactive PFKL cryo-EM structure, ligands were added to a final concentration of 2 mM ATP and 500 µM F16BP at pH 7.5. PFKM samples had ligands added at 1.7 mM ATP, 500 µM F16BP at pH 7.5 for the PFKM tetramer structure. PFKM dimer structures were done with ligands added at 4 mM ATP, 0.25 mM F6P, at pH:6.8. Cryo-EM data was collected on a FEI Titan Krios operating at 300 kV, using K3 Summit Direct Detector with a Gatan Image Filter (GIF). All datasets were collected using Legninon. For the inactive PFKL dataset, a subset of the data was collected at 30° to account for preferred orientation.

Data processing

Raw movies were motion corrected using MotionCorr2 (Relion 3.1[23]) and binned by 2. Motion corrected micrographs were then imported to Cryosparc[24] and CTFFind4 and Patch CTF (Cryosparc v.3) were used to estimate the CTF. Particle picking was performed using Blob Picker,

and particles were then extracted from micrographs. For the dimer PFKM dataset, a subset of particles was manually picked and then 2D classified to be used for templates for the Blob Picker, due to the small size of the protein. 3 rounds of 2D classification were performed after particle picking, removing noise and misaligned particles. For the dimer PFKM structure, 2D class averages were used to generate an *ab initio* reconstruction before continuing to C1 homogenous refinement in Cryosparc. For the inactive PFKL and tetramer PFKM datasets, particles were imported back to Relion for 3D reconstruction. For these structures, a reference model of the previously solved active PFKL tetramer or filament was used as a reference for an initial 3D refinement with C1 symmetry. Multiple rounds of masked 3D refinement were then performed with D2 symmetry for tetramer reconstructions and C2 symmetry imposed for filament structures. Unmasked 3D classification was used to further purify tetramers from filaments. Bayesian polishing, optics correction, and density modification (Phenix) were performed at the end of the data processing. Atomic models were built using ISOLDE (v.1.2) and Chimerax (v.1.3).

Preparing PFKL Construct for Expi293F Expression

Human PFKL DNA sequence was synthesized by Twist Bioscience into a pTwist plasmid with a CMV promoter. A twin step strep tag was added to the N terminus of PFKL followed by a TEV protease cleavage site. The dried down DNA was resuspended in nuclease free Tris-EDTA (TE) buffer, pH 8.0 at a final concentration of 100 ng/µL and stored at -20°C, per the manufacturer's instructions.

The pTwist-PFKL construct was transformed into Top10 competent cells. 3 µL of plasmid DNA were added to cells, which then incubated on ice for 30 minutes. Cells were then heat shocked for 30 seconds at 42°C and immediately left to recover on ice for 2 minutes. 250 µL of SOC medium were added and cells were left to recover at 37°C while shaking a 250 rpm for 1 hour. 50 µL of

cells were plated on carbenicillin agar plates. The plates were left overnight in a 37°C incubator. Colonies were then picked and inoculated into 5 mL cultures with 50 µg/mL carbenicillin. The pTwist-PFKL construct was then purified following the Quick Plasmid Miniprep Kit (Thermo Fisher) and sequenced using Genewiz using designed sequencing primers. For transfection purposes, maxi preps were performed using the Plasmid DNA Maxi Prep Kit (Thermo Fisher).

Transfection of PFKL into Expi293F Cells

We thank Brad Webb for supplying us with purified PFKL, PFKM, and PFKP protein stocks, prepared using a baculovirus system as described previously[14] for all cryo-EM and negative stain-EM experiments.

For human cell expression, we used Expi293F^{TM} cells (Thermo Fisher Scientific). Suspension Expi293F cells were passaged in Expi293 medium. Cell viability and concentration was assessed via Trypan Blue staining and counted using the Countess (Invitrogen). Cells were grown at 37°C, while shaking at 250 rpm with 8% CO_2. Shake flask cultures of 140 mL were used for cell expression and cells were harvested (spun at 300 x g at 4 °C for 20 minutes) three days post transfection. Transfection of cells took place over the course of two days. On the first day, cells were diluted to 2-2.5x10^6 cells/mL. The next day, cell viability was assessed, and cells were diluted to 3 x10^6/mL with warmed fresh Expi293 media. One mixture of OptiMEM (Thermo Fisher Scientific) and PFKL DNA to be transfected along with one mixture of the transfection agent, PEI (polyethylenimine) and OptiMEM at ratios as described by the manufacturer. These two reactions were then left at room temperature for 15 minutes, before being combined, and added to Expi293F cultures in a drop wise manner.

Protein Purification of PFKL from Expi293F Cells

Cell pellets were thawed on ice resuspended in a lysis buffer (20 mM Hepes, pH 7.5, 80 mM Potassium Phosphate,1 mM 2-mercaptoethanol, 10% glycerol) with one cOmplete^{TM} EDTA Free Protease Inhibitor Cocktail tablet (Roche). Cells were then lysed by addition of 1% Triton and incubation on ice for 30 minutes. The soluble lysate was then cleared by centrifugation (Lynx centrifuge, 13,000 rpm for 30 minutes at 4 °C) and then purified by a step-Tactin affinity chromatography column at 4 °C. The strep column was washed (20 mM Hepes pH 7.5, 1 mM DTT, 500 µM Ammonium Sulfate, 5% glycerol, 1 mM ATP, and 100 µM EDTA) with 5 column volumes. The PFKL protein was eluted in 20 mL of elution buffer (20 mM Hepes pH 8, 1 mM DTT, 500 µM Ammonium Sulfate, 5% glycerol, 1 mM ATP, 100 µM EDTA, 50 mM Biotin). The eluent was then incubated with TEV protease (1:100 TEV: PFKL) overnight while gently shaking at 4°C. The next day, a nickel column was set up at 4 °C and washed (20 mM Hepes pH 7.5, 1 mM DTT, 500 µM Ammonium Sulfate, 5% glycerol, 1 mM ATP, and 100 µM EDTA, 75 mM Imidazole). The overnight TEV mixture with the eluent was then added to the column to trap the his-tagged TEV protease onto the nickel beads. The eluent was then concentrated (Millipore Amicon Ultra 30K MWCO) and then further purified by size exclusion chromatography using an Äkta Pure (Cytivia Life Sciences) with a pre-equilibrated Superose 6 Increase column (20 mM Hepes, pH 7.5, 1 mM DTT, 500 µM Ammonium Sulfate, 5% glycerol, 1 mM ATP, 100 µM EDTA). A 4-15% SDS-PAGE gradient gel was run on SEC fractions at 180V for 45 minutes to confirm purity of the sample, to which 2X SDS dye was added to. The purified PFKL protein was then snap frozen with liquid nitrogen and then stored at -80°C.

Western Blot Analysis

Prior to protein purification, expression of PFKL in Expi293F cells were monitored via western blot analysis. Over the course of 3-, 4-, and 5-days post transfection, a 1 mL aliquot of cells was isolated. The aliquots were centrifuged (300 x g for 5 minutes at room temperature) and the supernatant discarded. Cell pellets were then resuspended in lysis buffer (20 mM Tris-HCl, pH 7.5, 50 mM potassium phosphate, 1 mM 2-mercaptoethanol, 10% glycerol, 10 mM imidazole) and then lysed with 1% Triton. The soluble lysate was then isolated via centrifugation (17,000 rpm for 5 minutes at room temperature). 2X SDS buffer was added to the samples and boiled for 2 minutes before loading onto a 4-15% SDS-PAGE gradient gel. The gel was run at 180V for 45 minutes. Proteins were transferred to a nitrocellulose membrane using a wet tank transfer system. The wet tank was stored at 4°C for 60 minutes while running at 100 V. Following membrane transfer, the nitrocellulose paper was washed with blocking buffer (Licor) at room temperature for 1 hour. The membrane was then incubated overnight at 4°C with primary anti-strep antibody (1:2000). The next day the membrane was washed four times with PBST (phosphate-buffered saline with Tween 20) with 5-minute incubation between each wash at room temperature while shaking. Next the membrane was then incubated with the secondary antibody (Goat, Polyclonal, Anti-Mouse IgG Conjugated to IRDye 800CW) for 1 hour at room temperature at a 1:2500 dilution. After this the membrane was washed four times with PBST with 5-minute incubation between each wash at room temperature while shaking. Lastly, the membrane paper was washed 2 times with diH_2O before imaging on a Licor Scanner.

Negative stain-EM

Negative stain samples were prepared by adding PFKL and PFKM to glow discharged carbon-coated grids using 0.7% uranyl formate. For the human expressed PFKL, 120 nM of protein was

loaded onto the grid. For all PFKM samples, 600 nM of protein was used with the appropriate concentrations of ligands used with the following concentrations: 4 mM ATP, 0.25 mM F6P, and 500 µM F16BP. For all negative stain grids, 3 µL of sample was pipetted onto glow discharged grids and were allowed to sit at room temperature for 1 minute. The protein was then blotted away with Whatman paper and immediately washed and blotted two times with diH_2O. After the last wash with water, 0.7% uranyl formate was immediately added to the grid and allowed to sit for 1minute. The uranyl formate was then carefully wicked away using Whatman paper. Imaging was done on a FEI Morgagni using an accelerating voltage of 100 kV.

REFERENCES

[1] Chaturvedi S, Singh AK, Keshari AK, Maity S, Sarkar S, Saha S. Human Metabolic Enzymes Deficiency: A Genetic Mutation Based Approach. *Scientifica* (Cairo). 2016;2016:9828672. doi:10.1155/2016/9828672

[2] Climent F, Roset F, Repiso A, Pérez de la Ossa P. Red cell glycolytic enzyme disorders caused by mutations: an update. *Cardiovasc Hematol Disord Drug Targets*. 2009;9(2):95-106. doi:10.2174/187152909788488636

[3] Yu L, Chen X, Sun X, Wang L, Chen S. The Glycolytic Switch in Tumors: How Many Players Are Involved?. *J Cancer*. 2017;8(17):3430-3440. Published 2017 Sep 20. doi:10.7150/jca.21125

[4] Peter M. Fernandes, James Kinkead, Iain McNae, Paul A.M. Michels, Malcolm D. Walkinshaw; Biochemical and transcript level differences between the three human phosphofructokinases show optimization of each isoform for specific metabolic niches. *Biochem J*. 2020; 477 (22): 4425–4441. doi: https://doi.org/10.1042/BCJ20200656

[5] Shirakihara Y, Evans PR. Crystal structure of the complex of phosphofructokinase from Escherichia coli with its reaction products. *J Mol Biol*. 1988;204(4):973-994. doi:10.1016/0022-2836(88)90056-3

[6] Schirmer T, Evans PR. Structural basis of the allosteric behavior of phosphofructokinase. *Nature*. 1990 Jan 11;343(6254):140-5. doi: 10.1038/343140a0. PMID: 2136935.

[7] Evans PR, Farrants GW, Hudson PJ. Phosphofructokinase: structure and control. *Philos Trans R Soc Lond B Biol Sci*. 1981 Jun 26;293(1063):53-62. doi: 10.1098/rstb.1981.0059. PMID: 6115424.

[8] Martínez-Costa OH, Hermida C, Sánchez-Martínez C, Santamaría B, Aragón JJ. Identification of C-terminal motifs responsible for transmission of inhibition by ATP of mammalian phosphofructokinase, and their contribution to other allosteric effects. *Biochem J*. 2004;377(Pt 1):77-84. doi:10.1042/BJ20031032

[9] Poorman, R., Randolph, A., Kemp, R. *et al.* Evolution of phosphofructokinase—gene duplication and creation of new effector sites. *Nature.* 1984; 309:467–469. doi: 10.1038/309467a0

[10] Lynch, EM et al. "Filament formation by metabolic enzymes-A new twist on Regulation." *Current opinion in cell biology*. 2020; 66: 28-33. doi:10.1016/j.ceb.2020.04.006

[11] Johnson MC, Kollman JM, Cryo-EM structures demonstrate human IMPDH2 filament assembly tunes allosteric regulation *eLife*. 2020; 9: e53243 doi: 10.7554/eLife.53243

[12] Hansen JM, Horowitz A, Lynch EM, Farrell DP, Quispe J, DiMaio F, Kollman JM, Cryo- EM structures of CTP synthase filaments reveal mechanism of pH-sensitive assembly during budding yeast starvation *eLife*. 2021;10:e73368.

[13] Lynch EM, Hicks DR, Shepherd M, Endrizzi JA, Maker A, Hansen JM, Barry RM, Gitai Z, Baldwin EP, Kollman JM. Human CTP synthase filament structure reveals the active enzyme conformation. *Nat Struct Mol Biol*. 2017 Jun;24(6):507-514. doi: 10.1038/nsmb.3407. Epub 2017 May 1. PMID: 28459447; PMCID: PMC5472220.

[14] Webb BA, Dosey AM, Wittmann T, Kollman JM, Barber DL. The glycolytic enzyme phosphofructokinase-1 assembles into filaments. *J Cell Biol*. 2017;216(8):2305-2313. doi:10.1083/jcb.201701084

[15] Webb, Bradley A et al. “Structures of human phosphofructokinase-1 and atomic basis of cancer-associated mutations.” *Nature* vol. 523,7558 (2015): 111-4. doi:10.1038/nature14405
[16] Amara N, Cooper MP, Voronkova MA, Webb BA, Lynch EM, Kollman JM, Ma T, Yu K, Lai Z, Sangaraju D, Kayagaki N, Newton K, Bogyo M, Staben ST, Dixit VM. Selective activation of PFKL suppresses the phagocytic oxidative burst. *Cell*. 2021 Aug 19;184(17):4480-4494.e15. doi: 10.1016/j.cell.2021.07.004. Epub 2021 Jul 27. PMID: 34320407; PMCID: PMC8802628
[17] Sola-Penna, M., Da Silva, D., Coelho, W.S., Marinho-Carvalho, M.M. and Zancan, P. (2010), Regulation of mammalian muscle type 6-phosphofructo-1-kinase and its implication for the control of the metabolism. *IUBMB Life*, 62: 791-796. doi: 10.1002/iub.393
[18] Banaszak K, Mechin I, Obmolova G, et al. The crystal structures of eukaryotic phosphofructokinases from baker's yeast and rabbit skeletal muscle. *J Mol Biol*. 2011;407(2):284-297. doi:10.1016/j.jmb.2011.01.019
[19] Trivedi B, Danforth WH. Effect of pH on the kinetics of frog muscle phosphofructokinase. *J Biol Chem*. 1966 Sep 10;241(17):4110-2. PMID: 4224144.
[20] Manoli SS, Kisor K, Webb BA, Barber DL. Ethyl isopropyl amiloride decreases oxidative phosphorylation and increases mitochondrial fusion in clonal untransformed and cancer cells. *Am J Physiol Cell Physiol*. 2021 Jul 1;321(1):C147-C157. doi: 10.1152/ajpcell.00001.2021. Epub 2021 May 26. PMID: 34038242; PMCID: PMC8321791.
[21] Lynch, E.M., Kollman, J.M. Coupled structural transitions enable highly cooperative regulation of human CTPS2 filaments. *Nat Struct Mol Biol*. 2020; 27:42–48. doi: 10.1038/s41594-019-0352-5
[22] Costa Leite T, Da Silva D, Guimarães Coelho R, Zancan P, Sola-Penna M. Lactate favors the dissociation of skeletal muscle 6-phosphofructo-1-kinase tetramers down-regulating the enzyme and muscle glycolysis. *Biochem J*. 2007 Nov 15;408(1):123-30. doi: 10.1042/BJ20070687. PMID: 17666012; PMCID: PMC2049071.
[23] Scheres SH. RELION: implementation of a Bayesian approach to cryo-EM structure determination. *J Struct Biol*. 2012 Dec;180(3):519-30. doi: 10.1016/j.jsb.2012.09.006. Epub 2012 Sep 19. PMID: 23000701; PMCID: PMC3690530.
[24] Punjani, A., Rubinstein, J., Fleet, D. *et al.* cryoSPARC: algorithms for rapid unsupervised cryo-EM structure determination. *Nat Methods*. 2017; 14:290–296. doi: 10.1038/nmeth.4169